2D Computation and Measurement of Electric and Magnetic Fields of Overhead Electric Power Lines

Slavko Vujević[1], Dino Lovrić[1] and Tonći Modrić[1]
[1]University of Split, Faculty of Electrical Engineering, Mechanical Engineering and Naval Architecture, Split, Croatia
vujevic@fesb.hr, dino.lovric@fesb.hr, tonci.modric@fesb.hr

***Abstract*—In this paper a 2D numerical algorithm is presented for the computation of electric and magnetic fields of power lines. The numerical algorithm for the electric field intensity computation takes into account a short power line and approximates the conductor charge density by a constant. The numerical algorithm for magnetic flux density computation is based on the application of the Biot-Savart law. The computed results are compared to measurements taken underneath a 400 kV power line. The computed results and measurements prove to be in good agreements keeping in mind that the sag of the power line section is approximated with a horizontal straight line. Both the computed results as well as measurements confirm the fact that the electric and magnetic fields of high voltage power lines are well within the prescribed limits.**

Keywords—electric field; magnetic field; overhead power line;measurement; 2D algorithm

I. INTRODUCTION

The possible adverse health effects produced by extremely low-frequency electric and magnetic fields of overhead electric power lines are a matter of certain controversy among researchers. The most feared public health effects are those of a carcinogenic nature, such as childhood leukemia. Numerous studies were conducted concerning this relationship, and limited evidence was found to confirm this hypothesis whereas for other forms of cancer, the evidence found was inadequate [1]. Generally, the reference occupational exposure levels recommended by ICNIRP guidelines [2] for 50 Hz are 500 μT for the magnetic flux density and 10 kV/m for the electric field intensity. As for the general public exposure to 50 Hz electric and magnetic fields, the reference levels are 100 μT for the magnetic flux density and 5 kV/m for the electric field intensity.

In numerical models for computing the power frequency electromagnetic field, the problem can be considered as quasi-static [3]. Quasi-static fields have the same spatial patterns as static fields, but vary slowly with time. Therefore, electric and magnetic fields may be computed separately.

Numerical algorithms for computing power frequency electric and magnetic fields in substations are three-dimensional (3D) algorithms. On the other hand, most of numerical algorithms for computing power line electric and magnetic fields are two-dimensional (2D) algorithms [4-9].

In this paper, numerical algorithms for computing the magnetic flux density and electric field intensity of finite power lines using 2D approximation of a power line will be presented [10]. The numerical algorithm for the electric field intensity computation takes into account a short power line and approximates the conductor charge density by a constant. This numerical algorithm proved to be optimal when compared to the algorithm which takes into account an infinite power line and the algorithm which takes into account a short power line, where the charge density is approximated by a parabola [10]. The numerical algorithm for magnetic flux density computation is based on the application of the well-known Biot-Savart law.

In order to investigate the suitability of 2D algorithms for computation of electric and magnetic fields of overhead power lines, measurements are taken underneath a 400 kV overhead power line and are compared to the results obtained by the presented 2D algorithms. The input data of the 400 kV overhead power line section as well as the measurement procedure and equipment are described in detail.

II. SCALAR ELECTRIC AND VECTOR MAGNETIC POTENTIALS

In 2D numerical algorithms for the computation of the electric and magnetic fields of a straight power line, conductors of the power line satisfy a thin-wire approximation and are treated as line sources positioned parallel to the earth surface [4-6]. The number of line sources equals the number of power line conductors, which are positioned in the air or earth at a constant distance from the earth surface. Line sources are oriented along the *x*-axis of the Cartesian coordinate system (Fig. 1). The origin of the selected coordinate system is on the earth surface and in the middle of the power line section. Cross sections of a typical three-phase high voltage power line with a single shield wire, arranged in the *x-z* plane of the selected coordinate system are presented in Fig. 1. Computation of the electric field intensity and magnetic flux density are carried out in the *y-z* plane, positioned in the middle of the power line section (Fig. 1).

According to the adopted thin-wire approximation, the conductor time-harmonic current flows along the conductor axis, and the conductor time-harmonic charge is located along the segment axis.

The starting point in the development of the mathematical model for the computation of electric and magnetic fields of power lines can be seen in solutions of the Helmholtz differential equation for the scalar electric and vector magnetic potentials [11]. In a homogeneous, linear, isotropic and unbounded medium, with neglected potential attenuation and phase shift effects, solutions of the Helmholtz equation for the scalar electric and vector magnetic potentials reduce to the solutions of the Poisson differential equations [3, 12, 13]. In the power frequency case, attenuation and phase shift effects can be neglected without loss of accuracy.

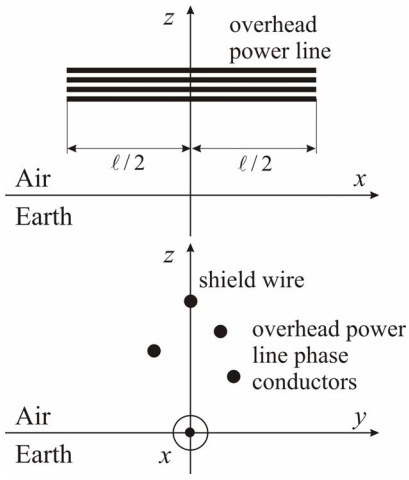

Figure 1. Position of an overhead power line in the *x*-*z* and *y*-*z* coordinate system

In the case of an arbitrary number of overhead power line conductors (*n*), solutions of the Poisson differential equations for the scalar electric and vector magnetic potentials in the air can be expressed by [12]:

$$\overline{\varphi} = \frac{1}{4\cdot\pi\cdot\varepsilon_0}\cdot\sum_{i=1}^{n}\left[\int_{\Gamma_{Ai}}\frac{\overline{\lambda}_i}{R_{Ai}}\cdot d\ell_{Ai} + \overline{F}\cdot\int_{\Gamma_{Bi}}\frac{\overline{\lambda}_i}{R_{Bi}}\cdot d\ell_{Bi}\right] \quad (1)$$

$$\underline{\vec{A}} = \vec{i}\cdot\frac{\mu_0}{4\cdot\pi}\cdot\sum_{i=1}^{n}\overline{I}_i\cdot\int_{\Gamma_{Ai}}\frac{1}{R_{Ai}}\cdot d\ell_{Ai} \quad (2)$$

where $\overline{\varphi}$ is a phasor of the scalar electric potential, $\underline{\vec{A}}$ is a phasor of the vector magnetic potential, $\overline{\lambda}_i$ is a phasor of the i^{th} conductor charge density, $\overline{I}_i$ is a phasor of the i^{th} conductor current, R_{Ai} is the distance between the field point and a source point, R_{Bi} is the distance between the field point and a source image point and $\vec{i}$ is the unit vector. The integration path Γ_{Ai} in (1) and (2) is positioned along the i^{th} conductor axis, whereas the integration path Γ_{Bi} is positioned along the axis of the i^{th} conductor image in relation to the earth surface.

The constant $\mu_0 = 4\cdot\pi\cdot10^{-7}$ H/m is the vacuum permeability and $\varepsilon_0 = 8.854\cdot10^{-12}$ F/m is the vacuum permittivity. In order to compute the electric field intensity of an overhead power line, one needs to take into account the effects of the earth. In (1) and (2), this effect is accounted for using the reflection coefficient $\overline{F}$ derived for a point current source [14], which can be expressed as follows:

$$\overline{F} = \frac{j\cdot2\cdot\pi\cdot f\cdot\varepsilon_0 - (\sigma + j\cdot2\cdot\pi\cdot f\cdot\varepsilon_0\cdot\varepsilon_r)}{j\cdot2\cdot\pi\cdot f\cdot\varepsilon_0 + (\sigma + j\cdot2\cdot\pi\cdot f\cdot\varepsilon_0\cdot\varepsilon_r)} \quad (3)$$

where σ is the electrical conductivity of the earth, f is the current frequency and ε_r is the relative permittivity of the earth. For power line frequencies, this factor can be approximated with high accuracy by $\overline{F} = -1$ as a consequence of assumption that the earth conductivity is infinite.

III. 2D COMPUTATION OF POWER LINE ELECTRIC FIELD WITH CONSTANT CONDUCTOR CHARGE DENSITY

In this paper the computation method for the electric field involves the assumption that the conductor charge density can be accurately approximated by a constant. In [10], this method proved to be the optimal in comparison with a more complicated approach where the conductor charge density is approximated by a parabolic approximation.

Computation of the overhead power line electric field intensity can be sought through the well-known equation that combines the scalar electric potential and the vector magnetic potential [3]:

$$\underline{\vec{E}} = -\nabla\overline{\varphi} - j\cdot\omega\cdot\underline{\vec{A}} = \left\{\overline{E}_x, \overline{E}_y, \overline{E}_z\right\} \quad (4)$$

where $\underline{\vec{E}}$ is a phasor of the electric field intensity and $\omega = 2\cdot\pi\cdot f$ represents the angular frequency.

In the case of the 2D approximation of the overhead power line, the vector magnetic potential has only the *x*-component, while the scalar electric potential distribution is symmetric with respect to the *y*-*z* plane. Components of the electric field intensity for the overhead power line can be computed from the following expressions [10]:

$$\overline{E}_x = \overline{E}_x\big|_{x=0} = -j\cdot\omega\cdot\overline{A}_x = -j\cdot\omega\cdot\overline{A}\big|_{x=0} \quad (5)$$

$$\overline{E}_y = \overline{E}_y\big|_{x=0} = -\frac{\partial\overline{\varphi}(x,y,z)}{\partial y}\Big|_{x=0} = -\frac{\partial\overline{\varphi}(0,y,z)}{\partial y} \quad (6)$$

$$\overline{E}_z = \overline{E}_z\big|_{x=0} = -\frac{\partial\overline{\varphi}(x,y,z)}{\partial z}\Big|_{x=0} = -\frac{\partial\overline{\varphi}(0,y,z)}{\partial z} \qquad (7)$$

where the partial derivatives of the scalar electric potential feature prominently in the development of the y and z components.

The total effective (rms) value of the electric field intensity at the field point P can be computed using the following expression:

$$E = \sqrt{\left|\overline{E}_{\mathrm{x}}\right|^2 + \left|\overline{E}_{\mathrm{y}}\right|^2 + \left|\overline{E}_{\mathrm{z}}\right|^2} = \sqrt{E_x^2 + E_y^2 + E_z^2} \qquad (8)$$

where E_x, E_y and E_z are the effective (rms) values of the electric field intensity components.

The magnetic vector potential at the y-z plane, which is caused by the currents of n conductors, can be expressed as follows [10]:

$$\overline{A}\big|_{x=0} = \frac{\mu_0}{2\cdot\pi}\cdot\sum_{i=1}^{n}\bar{I}_i\cdot\ell n\frac{\sqrt{d_i^2+\frac{\ell^2}{4}}+\frac{\ell}{2}}{d_i} \qquad (9)$$

where ℓ is the length of the power line section and d_i is the shortest distance between the field point and the straight line passing through the i^{th} conductor axis:

$$d_i = \sqrt{(y-y_i)^2+(z-z_i)^2} \qquad (10)$$

where y_i and z_i are the coordinates of the i^{th} conductor.

In all cases, the phasors of conductor currents $\bar{I}_{\mathrm{i}}$ and the phasors of conductor potentials $\overline{\Phi}_i$ are the input data. The shield wire of the overhead power line is a special case of the power line conductor with $\bar{I}_i = 0$ and $\overline{\Phi}_i = 0$. In this 2D algorithm, conductor charge densities are approximated by a constant in such a way that:

$$\overline{\lambda}_i = \frac{\overline{Q}_i}{\ell} \quad ; \quad i = 1, 2, ..., n \qquad (11)$$

where $\overline{Q}_i$ is a phasor of the i^{th} conductor charge. Components of the electric field intensity for the short overhead power line can be computed using [10]:

$$\overline{E}_x = -\frac{j\cdot\omega\cdot\mu_0}{2\cdot\pi}\cdot\sum_{i=1}^{n}\bar{I}_i\cdot\ell n\frac{\sqrt{d_i^2+\frac{\ell^2}{4}}+\frac{\ell}{2}}{d_i} \qquad (12)$$

$$\overline{E}_y = -\frac{1}{4\cdot\pi\cdot\varepsilon_0\cdot\ell}\cdot\sum_{i=1}^{n}\left[\frac{\partial G(0,d_i)}{\partial d_i}\cdot\frac{\partial d_i}{\partial y} + \overline{F}\cdot\frac{\partial G(0,D_i)}{\partial D_i}\cdot\frac{\partial D_i}{\partial y}\right]\cdot\overline{Q}_i \qquad (13)$$

$$\overline{E}_z = -\frac{1}{4\cdot\pi\cdot\varepsilon_0\cdot\ell}\cdot\sum_{i=1}^{n}\left[\frac{\partial G(0,d_i)}{\partial d_i}\cdot\frac{\partial d_i}{\partial z} + \overline{F}\cdot\frac{\partial G(0,D_i)}{\partial D_i}\cdot\frac{\partial D_i}{\partial z}\right]\cdot\overline{Q}_i \qquad (14)$$

where:

$$\frac{\partial G(0,v)}{\partial v} = -2\cdot\frac{\ell}{v}\cdot\frac{1}{\sqrt{4\cdot v^2+\ell^2}} \quad ; \quad v\in\{d_i, D_i\} \qquad (15)$$

In (13) and (14), the conductor charges $\overline{Q}_i$ are unknown and can be computed by solving the system of linear equations (A3) derived in Appendix A.

IV. 2D COMPUTATION OF POWER LINE MAGNETIC FIELD

Numerical algorithm for the computation of the magnetic flux density of the overhead power line is based on the application of the Biot-Savart law [3]. The situation of the arbitrary i^{th} phase conductor of the high voltage power line, positioned in the x direction of the selected coordinate system, is depicted in Fig. 2. In the numerical model, the conductor current $\bar{I}_i$ flows along the phase conductor axis and thus generates the magnetic field at the field point P(0, y, z) in the y-z plane, also depicted in Fig. 2.

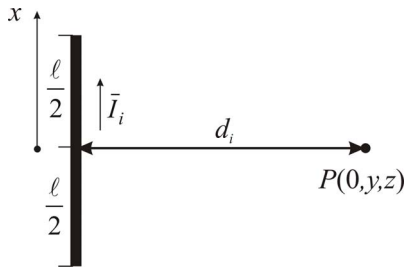

Figure 2. Computation of the magnetic field caused by a single-phase conductor of the power line

For a short power line, the components of the magnetic flux density are computed at the field point P(0, y, z) in the y-z plane using the following expressions [10]:

$$\overline{B}_x = 0 \qquad (16)$$

$$\overline{B}_{\mathrm{y}} = \mu_0 \cdot \sum_{i=1}^{n} \frac{(z_i - z)\cdot \ell}{4\cdot\pi\cdot d_i^2 \cdot \sqrt{d_i^2 + \frac{\ell^2}{4}}} \cdot \bar{I}_{\mathrm{i}}^{\ell} \tag{17}$$

$$\overline{B}_{\mathrm{z}} = \mu_0 \cdot \sum_{i=1}^{n} \frac{(y - y_i)\cdot \ell}{4\cdot\pi\cdot d_i^2 \cdot \sqrt{d_i^2 + \frac{\ell^2}{4}}} \cdot \bar{I}_{\mathrm{i}}^{\ell} \tag{18}$$

Finally, the total effective (rms) value of the magnetic flux density at the field point P can be written as:

$$B = \sqrt{\left|\overline{B}_{\mathrm{y}}\right|^2 + \left|\overline{B}_{\mathrm{z}}\right|^2} = \sqrt{B_y^2 + B_z^2} \tag{19}$$

V. Measuring Equipment and Measurement Procedure

The measurements of the electric and magnetic fields of the overhead power line were taken on a clear winter day (10 °C) in the middle of a 400 kV overhead power line section where the sag is greatest (Fig. 3 and Fig. 4). The terrain underneath the power line section was mostly clear except for some sporadic bushes (maximum height of 1.5 m). Computation and measurement of the electric and magnetic fields were carried out at field points along the *y*-directed profile, positioned at 1 m above the earth surface (z = 1 m).

The 400 kV overhead power line consists of three phases (L1, L2 and L3), with two conductors in the bundle per phase, and two shield wires (SW1 and SW2) in horizontal disposition (Fig. 3 and Fig. 4). The input data is given in Table I including the geometry as well as the current and potential phasors at the time when measurements were taken (obtained from the power company). Phase conductors are of type AlFe 490/65, whereas the shield wires are of type Alumweld 19/9. This yields the following radii of phase conductors $r_{01\text{-}06}$ = 15.30 mm and shield wires $r_{07\text{-}08}$ = 9 mm. Power line frequency f = 50 Hz, the length of the power line section ℓ = 376 m, relative permittivity of earth ε_r = 10 and electrical conductivity σ = 0.1 S/m.

TABLE I. Input Data of the 400 kV Overhead Power Line

	i	y (m)	z_s (m)	$\overline{\varphi}_i$ (kV)	$\bar{I}_i$ (A)
L1	1	-10.7	12.58	234.4∠0º	228∠-4.2º
	2	-10.4	12.58	234.4∠0º	228∠-4.2º
L2	3	-0.15	12.58	234.4∠240º	228∠235.8º
	4	0.15	12.58	234.4∠240º	228∠235.8º
L3	5	10.4	12.58	234.4∠120º	228∠115.8º
	6	10.7	12.58	234.4∠120º	228∠115.8º
SW1	7	-7.44	19.09	0∠0º	0∠0º
SW2	8	7.44	19.09	0∠0º	0∠0º

The z_s values in Table I are revised values of the real heights z of conductors due to sag. Catalogue data yield a sag of s = 11.43 m for phase conductors at 10 °C and s = 10.81 m for shield wires at 10 °C for a power line section of 380 m. The revised values are calculated by the following relation:

$$z_s = z - \frac{2}{3}\cdot s \tag{20}$$

A. Electric field intensity measurement

Considering the fact that, while taking the electric field measurement, the measurer **does** have a significant influence on the distribution of the electric field intensity, the measurement was taken at a 1 m height according to Fig. 3. The measurer must have a distance of a minimal 2 meters from the electric field meter in order to obtain an accurate reading of the instrument.

The electric field meter used was a Monroe Electronics Model 238A-1 AC Fieldmeter. The measuring probe was used to eliminate the distortion of electric field by the measurer.

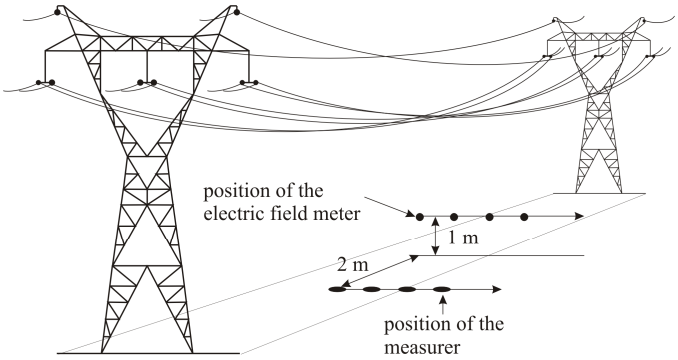

Figure 3. Measurement of the electric field intensity

B. Magnetic flux density measurement

Considering the fact that while taking the magnetic flux density measurement, the measurer **does not** have significant influence on the distribution of the magnetic flux density, the measurement was taken at a 1 m height according to Fig. 4.

The magnetic field meter used was a Sypris Triaxial ELF Magnetic Field Meter Model 4090.

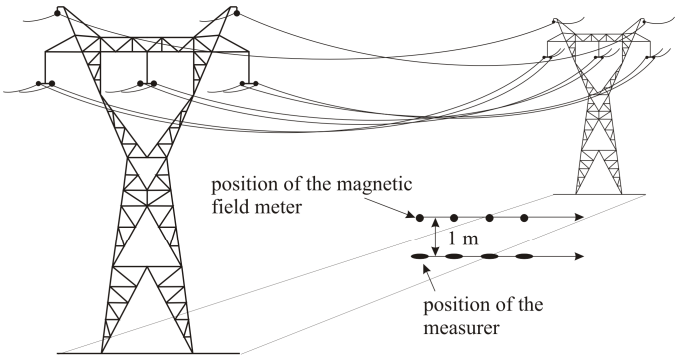

Figure 4. Measurement of the magnetic flux density

VI. COMPARISON OF MEASURED AND COMPUTED RESULTS

A. *Electric field intensity measurement*

In total, 23 measurements of the electric field intensity were taken at various distances from the middle of the overhead power line section. Naturally, since the rate of change of electric field intensity is greatest in the vicinity of the overhead power line which was accurately predicted by the 2D numerical algorithm, larger amount of measurements were taken in that area (Table II and Fig. 5). Table II presents measurements of the electric field intensity at the selected field points for easier reference. Notice that when the distance of the field point becomes larger than 40 m, the sensitivity of the instrument can not detect the electric field more accurately.

As can be observed from Table II and Fig. 5, it can be concluded that the computed and measured results of the electric field intensity are in good agreement. The main reason for deviations lies in the fact that the sag of the overhead power line was approximated by a straight line in the 2D numerical algorithm. Despite this, it can be concluded that the presented 2D algorithm yields satisfactory results.

TABLE II. MEASUREMENTS OF THE ELECTRIC FIELD INTENSITY

y (m)	E (kV/m)	y (m)	E (kV/m)
0	3.7	22	2
1	3.55	24	1.6
2	3.45	26	1.15
4	3.1	28	0.85
6	3.2	30	0.65
8	3.45	35	0.2
10	3.85	40	0.1
12	4	45	0.1
14	4.2	50	0.1
16	3.95	60	0.1
18	3.5	100	0.1
20	2.7		

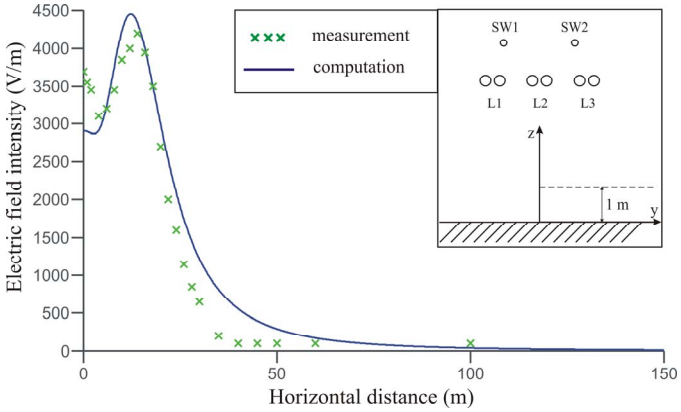

Figure 5. Comparison of measured and computed results of the electric field intensity beneath a 400 kV power line

B. *Magnetic flux density measurement*

In total, 20 measurements of the magnetic flux density were taken at various distances from the middle of the overhead power line section. Again, the field points were chosen based on the predicted shape of the magnetic flux density distribution computed by the 2D numerical algorithm (Table III and Fig. 6). Table III presents measurements of the magnetic flux density at the selected field points for easier reference.

As can be observed from Table III and Fig. 6, it can be concluded that the computed and measured results of the magnetic flux density are in better agreement than in the case of the electric field. Again, the reason for greatest deviations at $y = 0$ m lies in the fact that the sag of the overhead power line was approximated by a straight line in the 2D numerical algorithm. Despite this, it can be concluded that the presented 2D algorithm yields more than satisfactory results.

TABLE III. MEASUREMENTS OF THE MAGNETIC FLUX DENSITY

y (m)	B (μT)	y (m)	B (μT)	y (m)	B (μT)	y (m)	B (μT)
0	8.5	15	6.2	40	1.05	80	0.26
1	8.4	20	4.2	45	0.85	90	0.22
2	8.2	25	2.85	50	0.7	100	0.17
5	8.2	30	1.95	60	0.5	120	0.13
10	7.7	35	1.42	70	0.35	150	0.09

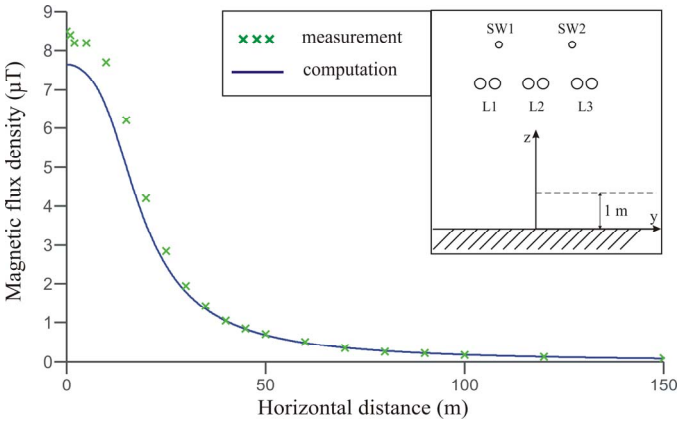

Figure 6. Comparison of measured and computed results of the magnetic flux density beneath a 400 kV power line

VII. CONCLUSION

In this paper, 2D algorithms for the computation of electric and magnetic fields of overhead power lines are presented. Presented algorithms are based on the thin-wire approximation. The sources of the magnetic fields are conductor currents, whereas the sources of the electric fields are conductor currents and conductor charge densities. The potential and current of the power line conductors are the input data, whereas the conductor charge densities are unknown.

The results computed by these 2D algorithms are compared to measurements taken underneath a 400 kV overhead power line. Bearing in mind that the overhead power line is approximated with a horizontal straight line, it can be concluded that good agreement was found between the computed results and measured results. However, more advanced 3D models are needed to accurately compute the electric and magnetic fields of more complicates structures such as electric power substations.

The computed results and measurements taken underneath a high voltage overhead power line both imply that the values of electric and magnetic fields are well within the limits prescribed by ICNIRP guidelines.

APPENDIX A. COMPUTATION OF CONDUCTOR CHARGES

The potential distribution in the *y*-z plane due to the conductor charges of all overhead power line conductors can be expressed by the following expression [10]:

$$\overline{\varphi}(0,y,z)=\frac{1}{4\cdot\pi\cdot\varepsilon_0\cdot\ell}\cdot\sum_{i=1}^{n}\left[G(0,d_i)+\overline{F}\cdot G(0,D_i)\right]\cdot\overline{Q}_i \qquad \text{(A1)}$$

where:

$$G(0,v)\;=\;2\cdot\sinh^{-1}\left(\frac{\ell}{2\cdot v}\right)\;\;;\;\; v\in\{d_i,\,D_i\} \qquad \text{(A2)}$$

The conductor charges can be computed by the well-known point collocation method with $x = 0$, which gives the following system of linear algebraic equations:

$$\sum_{i=1}^{n}\overline{Z}_{ji}\cdot\overline{Q}_i=\overline{\Phi}_j \quad ; \quad j=1,2,...,n \qquad \text{(A3)}$$

where $\overline{\Phi}_j$ is the potential of the j^{th} conductor collocation point.

According to (A1), (A2) and (A3), matrix coefficients $\overline{Z}_{ji}$ can be computed using the following expression:

$$\overline{Z}_{\text{ji}}=\overline{Z}(d_{ji})+\overline{F}\cdot\overline{Z}(D_{\text{ji}}) \qquad \text{(A4)}$$

where $\overline{Z}(d_{ji})$ and $\overline{Z}(D_{ji})$ can be computed using the equation:

$$\overline{Z}(v)=\frac{1}{2\cdot\pi\cdot\varepsilon_0\cdot\ell}\cdot\ell\text{n}\frac{\sqrt{\ell^2+v^2}+\frac{\ell}{2}}{v} \qquad \text{(A5)}$$

by introducing instead of *v*:

$$d_{ii}=r_{0i}\;;\;\; D_{ii}=2\cdot z_i \qquad \text{(A6)}$$

$$d_{ij}=\sqrt{(y_i-y_j)^2+(z_i-z_j)^2}\quad ;\quad i\neq j \qquad \text{(A7)}$$

$$D_{ij}=\sqrt{(y_i-y_j)^2+(z_i+z_j)^2}\quad ;\quad i\neq j \qquad \text{(A8)}$$

REFERENCES

[1] Non-Ionizing Radiation, Part 1: Static and Extremely Low-Frequency (ELF) Electric and Magnetic Fields, *IARC Monographs on the Evaluation of Carcinogenic Risks to Humans*, vol. 80, 2002.

[2] ICNIRP Guidelines for Limiting Exposure to Time-Varying Electric, Magnetic and Electromagnetic Fields (up to 300 Hz), *Health Physics,* vol. 74, no. 4, pp. 494-522,1998.

[3] Haznadar Z., Štih Ž., Electromagnetic fields, Waves and Numerical Methods, IOS Press: Amsterdam, 2000.

[4] Moro F., Turri R., Fast analytical computation of power-line magnetic fields by complex vector method, *IEEE Transactions on Power Delivery*, vol. 23, no. 2, pp. 1042-1048, 2008.

[5] Kaune W.T., Zaffanella L.E., Analysis of magnetic fields produced far from electric power lines, *IEEE Transactions on Power Delivery,* vol. 7, no. 4, pp. 2082-2091, 1992.

[6] Memari A.R., Janischewskyj W., Mitigation of magnetic field near power lines, *IEEE Transactions on Power Delivery*, vol. 11, no. 3, pp. 1577-1586, 1996.

[7] Filippopoulos G., Tsanakas D., Analytical calculation of the magnetic field produced by electric power lines, *IEEE Transactions on Power Delivery* 2005, vol. 20, no. 2, pp. 1474-1482, 2005.

[8] Garrido C., Otero A.F., Cidrás J., Low-frequency magnetic fields from electrical appliances and power lines, *IEEE Transactions on Power Delivery*, vol. 18, no. 4, pp. 1310-1319, 2003.

[9] Olsen R.G., Deno D., Baishiki R.S. et al., Magnetic fields from electric power lines theory and comparison to measurements, *IEEE Transactions on Power Delivery*, vol. 3, no. 4, pp. 2127-2136., 1988.

[10] Vujević S., Lovrić D., Sarajčev P., Comparison of 2D algorithms for ther computation of power line electric and magnetic fields, *European Transactions on Electrical Power (ETEP)*, vol. 21, no.1, pp. 505-521, 2011.

[11] Moore J., Pizer R. (editors). Moment Methods in Electromagnetics - Techniques and Applications, New York: John Wiley & Sons, 1984.

[12] Sarajčev P. Electromagnetic model of the system of conductors in multilayer medium, (in Croatian), Ph.D. Thesis, University of Split, FESB, Split, 2008.

[13] Vujević S., Time-harmonic analysis of earthing grids, in *Electrical Engineering and Electromagnetics VI*, C. A. Brebbia and D. Poljak, Ed., Southampton, Boston: WIT Press, pp. 235-244, 2003.

[14] Vujević S., Sarajčev P., Potential distribution for a harmonic current point source in horizontally stratified multilayer medium, *COMPEL*, vol. 27, no. 3, pp. 624–637, 2008.